Geomechanics and Engineering, *Vol. 25, No. 4 (2021) 275-282*
DOI: https://doi.org/10.12989/gae.2021.25.4.275

Microstructural observations of shear zones at cohesive soil-steel interfaces under large shear displacements

Belgacem Mamen*[1] and Farid Hammoud[2a]

[1]*Department of Civil Engineering, Faculty of Science and Technology, University Abbés Laghrour of Khenchela, Algeria*
[2]*Department of Civil Engineering, Faculty of Technology, University Mustapha Ben Boulaid of Batna, Algeria*

(Received November 5, 2020, Revised April 11, 2021, Accepted April 27, 2021)

Abstract. Failure mechanism which can affect geotechnical infrastructures (shallow foundations, retaining walls, and piles) constitutes one of the most encountered problems during the design process. In this respect, the shear behavior of interfaces between grained soils and solid building materials, as well as those between cohesive soils should be investigated. Therefore, a range of ring shear tests with different cohesive soils and stainless-steel interfaces have been carried out through the Bromhead apparatus that allows simulating large displacements along a failure surface. The effects of steel rings roughness and soil type on the residual friction coefficient and the shear zone features (structure, thickness, and texture orientation angle) have been investigated using the Scanning Electron Microscopy. The obtained results indicate that the residual friction coefficient and the structural characteristics of the shear zone vary according to the surface roughness and the soil type. Scanning electron microscopy reveals that the particles inside the shear zone tend to be re-oriented. Also, the shear failure mechanism can be identified along with the interface, within the soil, or simultaneously at the interface and within the soil specimen.

Keywords: failure mechanism; Bromhead apparatus; large displacements; cohesive soils; shear zone features; surface roughness

1. Introduction

Many geotechnical infrastructures, including shallow foundations, retaining walls and piles, made of construction material are often surrounded by fine-grained soil. Knowledge of soil-construction material interface shear behavior is one of the most important steps in the geotechnical design process. Consequently, a variety of laboratory shear tests have been extensively conducted through direct shear or simple shear tests to explain the interface shearing between soil and different building materials used in construction (Morgenstern and Tchalenko 1969, Tsubakihara *et al.* 1993, Takizawa *et al.* 2005, Li *et al.* 2012, Feligha *et al.* 2015, Wu and Yang 2017, Lee *et al.* 2017, Han *et al.* 2019, Heidemann *et al.* 2020). These experimental results have improved understanding of fine-grained soils shear behavior, but they could not adequately show the shear characteristics of fine-grained soils under large shear displacements.

As compared to the conventional direct shear and the simple shear devices, ring shear apparatus allows unlimited shear deformation of the specimen and recreates in the laboratory exactly the field conditions. Therefore, ring shear apparatus has been widely used to assess the shear behavior of soil under significant shear displacements such as the residual strength characteristics (Lemos *et al.* 2000, Wan and Kwong 2002, Meehan *et al.* 2007, Kimura *et al.* 2013, Eid *et al.* 2015, Xu *et al.* 2018, Eid *et al.* 2019) and shear band characteristics (Hicher *et al.* 1995, Wafid Agung *et al.* 2004, Fukuoka *et al.* 2006, Torabi *et al.* 2007, Li and Aydin 2013, Suzuki *et al.* 2017). Significant literature points out that the shear zone evolution in soils at the microscopic level is commonly accompanied by the variations in the grain size distribution (Wang *et al.* 2002, Coop *et al.* 2004, Jiang *et al.* 2016), the grain contact (Grelle and Guadagno 2010), the grain orientation (Chen *et al.* 2014), and the grain shape (Sadrekarimi and Olson 2010, Wei *et al.* 2018).

However, only a limited amount of work has studied the shear zone evolution in fine grained-soils at the microscopic level through ring shear tests (Mandl *et al.* 1977, Lupini *et al.* 1981, Khosravi *et al.* 2013, Al-Bared *et al.* 2019, Wang et al 2020). Mandl *et al.* (1977) have investigated the structural evolution of shear zones and the accompanying changes in texture and stress state in granular material undergoing continued shearing. As a conclusion, the shear zone can be compactive or dilative. Lupini *et al.* (1981) have conducted ring shear tests to measure the drained residual strength of cohesive soils. Three shearing modes in this study have been identified: a turbulent mode, a sliding mode and a transitional mode. All those modes depended on the clay fraction (% < 2 μm) and the particle size. In order to illustrate the effect of the shear displacement rate on the measured shear strengths, the particle arrangement and the surface asperities of the shear surface, slow and fast ring shear tests have been conducted on pre-sheared discontinuities in kaolinite by Khosravi *et al.* (2013). According to the test results, the "threshold" and "fast

*Corresponding author, Associate Professor
E-mail: belgacem.mamen@univ-khenchela.dz
[a]Professor
E-mail: f.hammoud @univ-batna2.dz

http://www.techno-press.org/?journal=gae&subpage=7
ISSN: 2005-307X (Print), 2092-6219 (Online)

maximum" strengths were always higher than the "slow drained residual" strength, but the fast minimum residual strength could sometimes drop to a lower value, especially at lower effective normal stresses. Additionally, SEM observations of the failure surface obtained at lower and higher shear strengths indicated no significant difference in the particle arrangement and surface asperities of the shear surface. Finally, meaningful insights for understanding the shear zone structure in fine-grained soils subjected to large shear displacements were provided by Wang *et al.* (2020) through a series of drained ring shear tests and microscopic observation. The residual strength of the soil samples gradually decreased with increasing moisture content and shearing speed. Furthermore, increasing moisture content and shearing speed had positive impact on the concentration of clay fraction around the shear planes resulting in a smaller median grain size.

To improve the knowledge of the shear behavior of interfaces between fine-grained soils and solid building materials, the structure of shear zones in fine-grained soils is a primary consideration. A series of ring-shear tests have been performed in the present study using remolded samples subjected to different shearing stages to understand better the degree of variation in residual friction coefficient (RFC) of silt (S), Silt-Kaolin (SK), and Kaolin (K). Another concern is to find out the effect of steel rings roughness on the structure, the thickness as well as the texture orientation angle of the shear zone of the three different soils. Importantly, the Scanning Electron Microscopy (SEM) analysis is the main source of information in assessing these features.

2. Apparatus and test procedure

The Bromhead-type ring shear apparatus suitable for soil, as described in Hoyos *et al.* (2011), has been used in this study Fig. 1(a). Firstly, a recent study reports that the initial soil condition has no significant influence on residual strength, Li *et al.* (2017). Therefore, a sample in a remolded state has been used. Test specimen has been prepared by kneading evenly soil paste into the annular space in the Bromhead ring shear device, as shown in Fig. 1(b). The sample is obtained by mixing dry soil with distilled water at the liquid limit. After a certain mixing time, the ultimate random state is reached and the sample is then left to dry until it reaches a water content equivalent to 1.5 times the plastic limit approximately. Secondly, the samples have been initially consolidated under the constant normal pressure of 70 kPa. Following this, the specimens have been tested at a slow shear rate of 0.035 mm/min for 24 hours. By using this slow value, the excess pore pressure is completely dissipated during this stage. Once the shear rate is down to zero, the samples are re-sheared at 44.52 mm/min (stage 2). Finally, a slow shearing rate (0.035 mm/min) has been immediately performed after consolidation (stage 3). In this investigation, a particular emphasis is given to the behavior at a large displacement of the third slow shearing stage. The schematic representation of the test procedure is shown in Fig. 2. All the tests have been carried out according to the

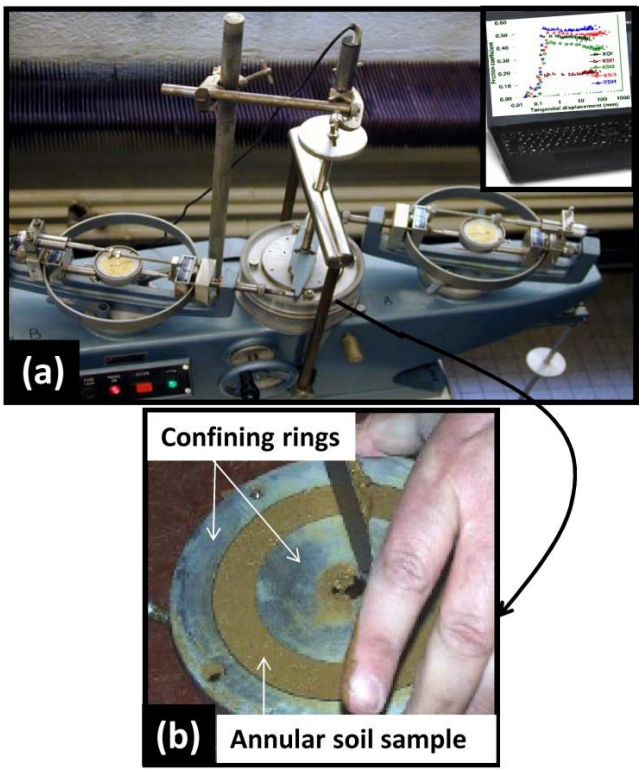

Fig. 1 (a) Illustration of the Bromhead ring shear device and (b) annular soil sample

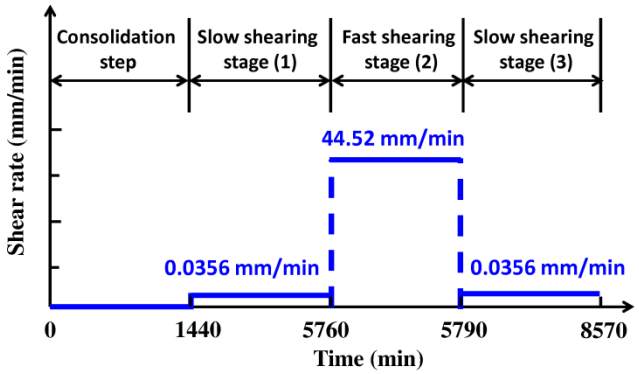

Fig. 2 Schematic representation of the test procedure

American Society for Testing and Materials (ASTM) guidance, ASTM D6467-13e1 (2013).

3. Used soils and interfaces

3.1 Used soils

The present experimental study is carried out on three kinds of cohesive soils having different clay fractions (% < 2 μm) and particle size distributions: silt (S), a mixture of silt and Kaolin (SK), and a clay called Kaolin (K). The primary mineral in this kaolin (K) is kaolinite with accessory minerals like mica, quartz, and Feldspar (Takizawa *et al.* 2005, Torabi *et al.* 2007, Mamen *et al.* 2018). The used silt (S) has been extracted from the Xeuilley area, located at Nancy North–West (France). The

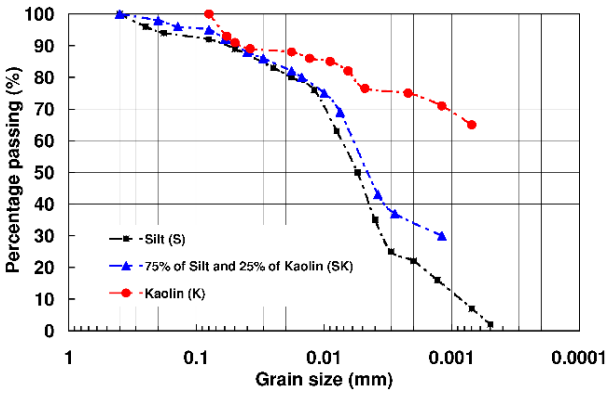

Fig. 3 Particle size distribution for silt (S), Silt-Kaolin (SK) and Kaolin (K)

Table 1 Basic properties of silt (K), Silt-Kaolin (SK) and Kaolin (K)

Geotechnical properties	S	SK	K
Liquidlimit, w_l(%)	53.40	45.60	64.50
Plastic limit, w_p (%)	39.90	34.00	32.20
Plasticity index, I_p (%)	13.50	11.60	32.30
Clay fraction (% < 2 µm)	22.00	34.00	76.00
Averagediameter, D_{av} (µm)	28.71	17.31	08.59
Specificgravity of solidparticles, G_s	02.68	02.67	02.64

X-ray diffraction analysis revealed that this silt contains 60% Quartz, 20 % Montmorillonite, 11% Feldspar, (4-5%) Kaolinite, and (4-5%) Mica. Finally, the SK consists of a mixture of 25% Kaolin and 75 % silt. As stated in the Unified Soil Classification System (USCS), the silt (S) is classified as MH, Kaolin as CH, and the mixture (SK) as ML. The particle size distribution curves of these soils have been determined according to the American Society for Testing and Materials (ASTM) guidance-D6913M-17 (2017), as shown in Fig. 3.

The soils' properties used in this investigation are summarized in Table 1. The liquid limit, the plastic limit, the plasticity index, and the density of solid particles are respectively determined according to ASTM-D4318-17e1 (2017) and D854-14 (2014).

3.2 Used interfaces

The experimental tests have been performed with original bronze ring (OI: original interface) for soil-soil interface, and stainless-steel rings (SI: steel interface) for soil-steel interfaces with varying roughness degrees (SI1: smooth interface, SI2-SI3: interfaces of intermediate roughness and SI4: rough interface). These rings have the same dimensions as the original ring and a sufficient thickness to spread the vertical charge uniformly, as shown in Fig. 4. The finished steel surface has been thoroughly cleaned by acetone before shearing tests. Also, the surface roughness measurements have been made using laser profilometer. Based on Eq. (1), the surface roughness data (Ra) of the four stainless steel interfaces is presented in Table 2.

$$R_a = \frac{1}{L}\int_0^L |Y(x)|dx \quad (1)$$

where L is the length sample and $Y(x)$ is the roughness profile ordinate, as shown in Fig. 5.

Table 2 Average surface roughness (Ra) of the used steel rings

Roughness parameter	SI	SI2	SI3	SI4
Ra (µm)	1.60	7.60	12.10	40.20

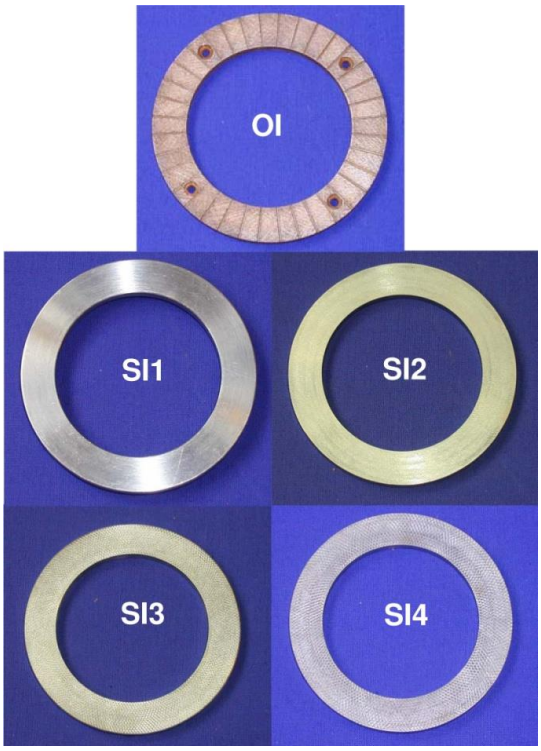

Fig. 4 Original bronze interface (OI) and stainless-steel interfaces with varying roughness (SI1-SI4)

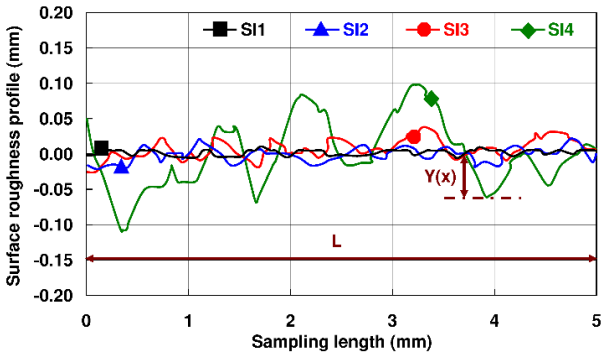

Fig. 5 Typical transverse section surface roughness profile of the used steel rings

4. Results and discussion

4.1 Evolution of friction coefficient

Figs. 6(a)-6(c) show the friction coefficient versus

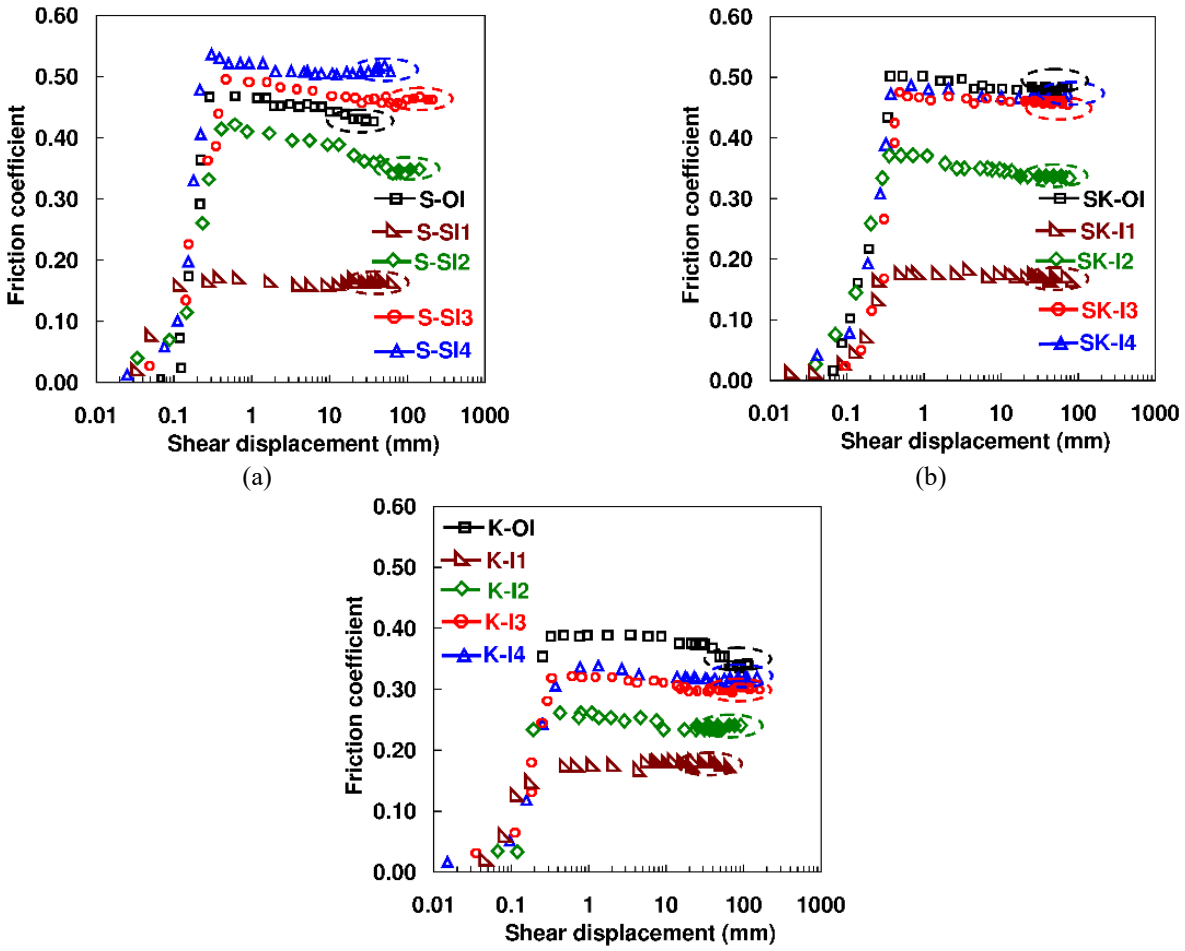

Fig. 6 Typical friction coefficient-shear displacement curves of the soils original interface (OI) and steel interfaces (SI1, SI2, SI3, and SI4), (a) the silt, (b) the Silt-Kaolin and (c) the Kaolin.

Table 3 Residual friction coefficient (RFC) for soil-soil and soil-steel interfaces

Interface type	Test (a)	RFC	Test (b)	RFC	Test (c)	RFC
Soil-soil	S-IO	0.420	SK-IO	0.480	K-IO	0.337
Soil-steel	S-SI1	0.156	SK-I1	0.178	K-SI1	0.150
	S-SI2	0.348	SK-I2	0.327	K-SI2	0.234
	S-SI3	0.464	SK-I3	0.456	K-SI3	0.297
	S-SI4	0.504	SK-I4	0.476	K-SI4	0.308

displacement curves obtained from shear tests using the original interface (OI) and different steel interfaces (I1-I4) for the silt (S), the Silt-Kaolin (SK), and Kaolin, respectively. It is noted that the largest increase in friction coefficient is generally obtained for steel interface SI4 having the highest average surface roughness (Ra=40.20), Table 2. One of the reasons for this behavior is that silt particles could closely fit into the asperities of the steel interface. Hence, better interaction between the soil specimen and steel ring surface occur. As the soil particles are big compared to the concavity of the asperities of SI1, the interaction between the soil specimen and steel ring surface is not sufficient leading to a lower friction coefficient, Figs. 6(a)-6(c).

Actually, the present study concerns the residual friction coefficient at large shear displacements. At this level, the friction coefficient exhibits a small decease which depends on the surface roughness. This small decrease can be related to the failure along with the interface. In this failure mode, the clay particles maintain a parallel face-to-face structure and tend to point toward the shear direction which increases the motion of steel plate moving with respect to the soil surface. As a result, the friction coefficient decreases with an increase in shear displacement. This tendency is consistent with the findings of Feligha *et al.* (2015) and Eid *et al.* (2015). Table 3 summarizes the obtained results in terms of residual friction coefficient (RFC) for soil-soil and soil-steel interfaces used in this investigation.

The fall in residual friction coefficient measured for

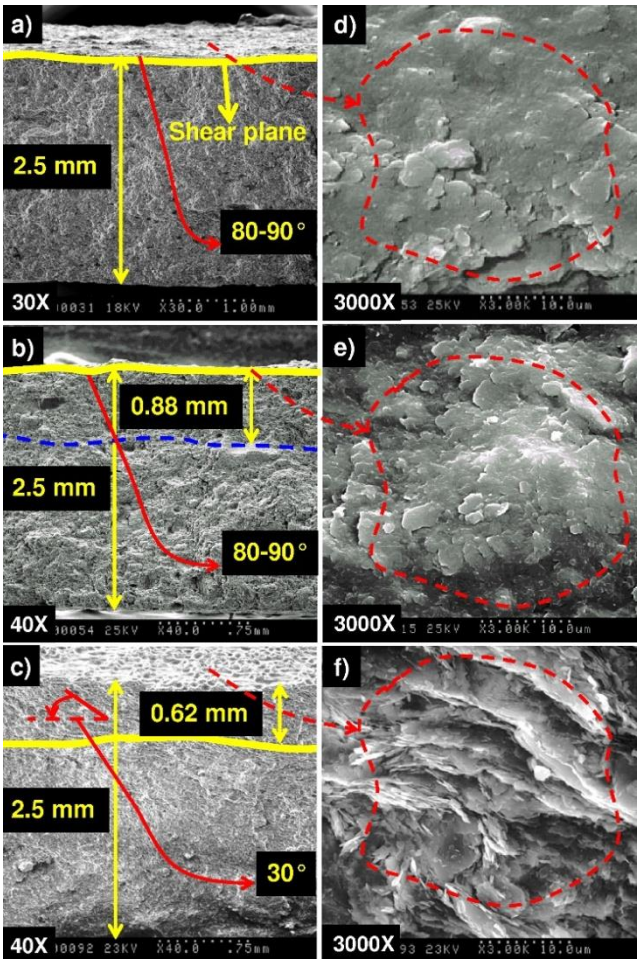

Fig. 7 Typical cross-sectional SEM micrographs showing the shear zone features using origin interface (OI). (a) Limon de Xeuilley (X), (b) Limon de Xeuilley-Kaolin (XK) and (c) Kaolin (K). (d) Failure plane created at the surface near the top of the silt sample in interfacial mode, (e) Failure plane created at the surface near the top of the silt-kaolin sample in interfacial mode and (f) Failure plane created within the kaolin sample in internal mode

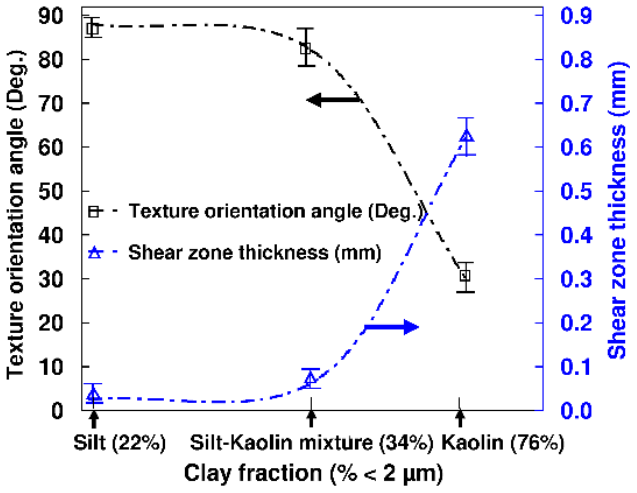

Fig. 8 Shear zone thickness and its texture orientation angle as a function of clay fraction (% < 2 µm)

kaolin, test (c) in Table 3, can be explained by the mineralogical composition of the soil. The soil mineral analysis shows that the predominant mineral for the silt and the mixture of silt-kaolin is Quartz while the predominant clay mineral in kaolin is kaolinite. Kaolinite particles have a diameter of about 1 µm and a thickness of 0.1 µm generating a smooth surface; and hence, a lower residual friction coefficient is obtained, Duong *et al.* (2018).

4.2 Interface behavior

4.2.1 Soil-soil

Several researchers have studied shear zones in reconstituted soils through various techniques such as optical and scanning electron microscopy (Morgenstern and Tchalenko, 1969, Mandl *et al.* 1977, Hicher *et al.* 1995, Thakur 2007, Chen *et al.* 2014, Jiang *et al.* 2016, Wang *et al.* 2020). Fig. 7(a) shows a cross-sectional SEM micrograph of the entire thickness of the silt sample (2.5 mm) after ring-shearing at large displacement. The soil fabric does not show any preferential orientation (80-90°), the texture is homogeneous and only particles near the interface surface are dispersed. Thus, indicating that an interfacial shear has taken place between the silt surface and the original interface.

Concerning the silt-kaolin sample shown in Fig. 7(b), the cross-sectional SEM micrograph reveals two zones with a different appearance. The final texture of the first zone, adjacent to the shear plane and extends about one-third of

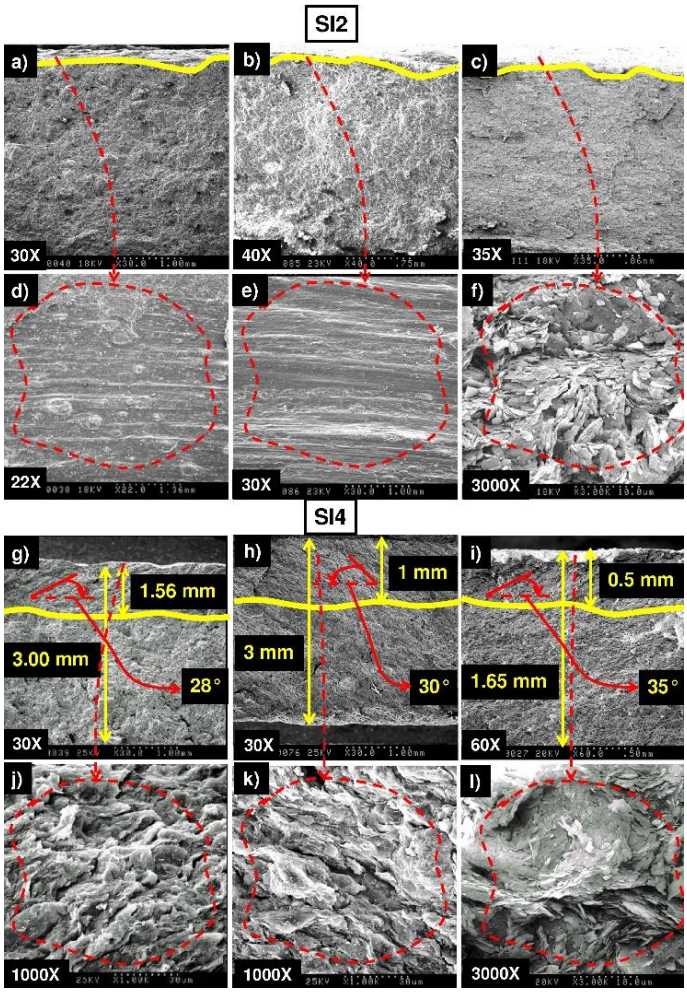

Fig. 9 Typical cross-sectional SEM micrographs of the soil samples. (a)-(g) Silt, (b)-(h) Silt-kaolin mixture and (c)-(i) Kaolin, using different steel interfaces SI2 and SI4

the thickness (0.88 mm), seems to be denser than the second one. Moreover, the scanning electron microscopy analysis for the silt and silt-kaolin samples as shown respectively in Figs. 7(a) and 7(b) reveal that the failure surface has not occurred inside the soil samples. This means that there is practically no shear zone and that the possible failure mode is interfacial (interface failure). At higher magnification of 3000 times in Figs. 7(d) and 7(e), the interface failure becomes more and more evident. Besides, kaolinite platelets, only at random spots, maintain a parallel face-to-face structure and tend to point toward the shear direction. Elsewhere, it is noted that the striations are prevented to be formed due to the presence of massive minerals' pockets.

Fig. 7(c) shows a cross-sectional SEM micrograph of the entire thickness of the kaolin sample (2.5 mm) after ring-shearing at large displacement. The surface impressions, shown on the shear face, are due to the upper porous ring. Fig. 7(c) also reveals that the clay particles outside the shear zone keep a random orientation. Inside (0.62 mm from the shear plane), the clay particles are oriented at an angle of about 30° with respect to the horizontal. Moreover, Fig. 7(f) shows a clear alignment of the streaked clay particles indicating that the failure plane has been created in the middle of the kaolin sample (internal failure). Thus, the present SEM micrographs support the hypothesis that soil composition plays a key role in the failure localization, Srivastava *et al.* (2020).

Fig. 8 displays the evolution of the shear zone thickness and its texture orientation angle as a function of clay fraction (% < 2 µm). The shear zone features evolution shows two different stages, each with its slop. The first one ends at 34%, the shear zone thickness and its texture orientation angle are nearly constant because of the full sliding at the interface (interface failure). In the second stage, a distinct increase of shear zone thickness and decrease in texture orientation angle are observed when clay fraction (% < 2 µm) exceeds 34 % indicating that the failure plane is created in the middle of kaolin sample (internal failure). These results confirm that the evolution of shear zones features is directly connected to the presence of clay fraction (% < 2 µm).

4.2.2 Soil-steel

The Scanning Electron Microscopy (SEM) analyses are the main source of information in assessing the shear zones at cohesive soil-steel interfaces under large displacements. From the data analysis, the shear failure mechanism can be identified along with the interface (interfacial), within the soil (internal) or simultaneously at the interface and within the soil specimen (intermediate).

For very smooth interfaces such as SI1, entire sliding is limited to the interface region in which particles are mobilized in the interaction. Visual inspections of samples obtained from tests S-SI1, SK-SI1, and K-SI1 show that the shear failure has occurred near the top of the soil samples in interfacial mode.

Considering the moderate roughness (SI2 and SI3), partial interface sliding and shear failure within the soil specimen occur simultaneously. This failure mode is called mixed or intermediate. On the one hand, the clay particles are inclined 40 to 50° from the horizontal within the shear zones and any deformation is localized, Figs. 9(a), 9(b) and 9(c). On the other hand, Figs. 9(d), 9(e) and 9(f) illustrate a well-defined slickensided shear surfaces because of the interface asperities. In this case, the macroscopic morphology of these shear surfaces shows undulations in the direction of shearing indicating that partial interface sliding appears simultaneously with the distortion inside the soil samples.

For rough interfaces (SI4), the distortion inside the soil samples takes place. Figs. 9(g), 9(h) and 9(i) show respectively cross-sectional SEM micrograph of the entire thickness of the silt (S), silt-kaolin (SK), and kaolin (K) samples. These cross-sectional SEM micrographs demonstrate two zones with a different appearance. The final texture of the first zone, which is adjacent to the shear plane and extends about one-third of the thickness seems to be denser than the second one. Within the first zone, all the structural elements are inclined between 28 and 35° from the horizontal. Additionally, the failure planes are created within the soil specimens and not at the soil interfaces. Figs. 9(j), 9(k), and 9(l) show three micrographs at higher magnification obtained after ring-shearing (SI4). They indicate that all particles along shear surfaces have the same orientation of shear. This orientation confirms that many particles in the sample tend to be involved in the shear failure mechanism.

5. Conclusions

In this paper, shear behavior of interfaces between grained soils and stainless-steel used in construction as well as those between cohesive soils has been investigated. The focus has been placed on analyzing the evolution of the residual friction coefficient and the shear zone features; structures, thickness, and texture orientation angle using SEM. Three different failure mechanisms have been identified along with the interface, within the soil or simultaneously at the interface and within the soil specimen.

Based on the SEM analysis regarding soil-soil failure, the formation of shear failure has been localized along a striated surface for silt and silt-kaolin samples. Also, the clay particles are formed by face-to-face which means that there is practically no shear zone and that the possible failure mode is an interfacial failure. However, the kaolin sample shows a 0.62 mm thick shear zone wherein the clay particles tend to be oriented in the shear direction with an angle of about 30 degrees from horizontal.

For soil-steel shearing, the failure plane has been created as a polished failure surface at the top of the soil samples for very smooth interfaces (SI1). In this case, only particles near the interface are dispersed; thus, indicating that a full sliding is limited to the interface. For interfaces of intermediate roughness like (SI2) and (SI3), the partial sliding occurs at the interface simultaneously with the distortion of clay fabric inside the soil samples. However, analysis of interface shearing with rough interfaces (SI4) shows a deep shear zone. Also, all the structural elements in this zone have the same orientation of shear. This orientation indicates that more particles in the sample tend to be involved in the shear failure mechanism.

Acknowledgments

The work presented in this paper has been supported by Abbès Laghrour University (Khenchela, Algeria) and Mustapha Ben Boulaid University (Batna, Algeria). Their support is gratefully acknowledged.

References

Al-Bared, M.A.M., Harahap, I.S.H, Marto, A., Alavi Nezhad Khalil Abad, S.V. and Montasir, O.A.A. (2019), "Undrained shear strength and microstructural characterization of treated soft soil with recycled materials", *Geomech. Eng.*, **18**(4), 427-437, http://doi.org/10.12989/gae.2019.18.4.427.

ASTM D4318-17e1 (2017), Standard Test Methods for Liquid Limit, Plastic Limit, and Plasticity Index of Doils, ASTM International, West Conshohocken, Pennsylvania, U.S.A.

ASTM D6467-13e1 (2013), Standard Test Method for Torsional Ring Shear Test to Determine Drained Residual Shear Strength of Cohesive Soils, ASTM International, West Conshohocken, Pennsylvania, U.S.A.

ASTM D6913M-17 (2017), Standard Test Methods for Particle-Size Distribution (Gradation) of Soils Using Sieve Analysis, ASTM International, West Conshohocken, Pennsylvania, U.S.A.

ASTM D854-14 (2014), Standard Test Methods for Specific Gravity of Soil Solids by Water Pycnometer, ASTM International, West Conshohocken, Pennsylvania, U.S.A.

Chen, J., Dai, F., Xu, L., Chen, S., Wang, P., Long, W. and Shen, N. (2014), "Properties and microstructure of a natural slip zone in loose deposits of red beds, southwestern China", *Eng. Geol.*, **183**, 53-64. http://doi.org/10.1016/j.enggeo.2014.10.004.

Coop, M.R., Sorensen, K.K., Bodas Freitas, T. and Georgoutsos, G. (2004), "Particle breakage during shearing of a carbonate sand", *Géotechnique*, **54**(3), 157-163, http://doi.org/10.1680/geot.2004.54.3.157.

Duong, N.T., Suzuki, M. and Van Hai, N. (2018), "Rate and acceleration effects on residual strength of kaolin and kaolin–bentonite mixtures in ring shearing", *Soils Found.*, **58**(5), 1153-1172. http://doi.org/10.1016/j.sandf.2018.05.011.

Eid, H.T., Al-Nohmi, N.M., Wijewickreme, D. and Amarasinghe, R.S. (2019), "Drained peak and residual interface shear strengths of fine-grained soils for pipeline geotechnics", *J. Geotech. Geoenviron. Eng.*, **145**(10), 06019010. http://doi.org/10.1061/(ASCE)gt.1943-5606.0002131.

Eid, H.T., Amarasinghe, R.S., Rabie, K.H. and Wijewickreme, D. (2015), "Residual shear strength of fine-grained soils and soil–solid interfaces at low effective normal stresses", *Can. Geotech. J.*, **52**(2), 198-210. https://doi.org/10.1139/cgj-2014-0019.

Feligha, M., Hammoud, F., Belachia, M. and Nouaouria, M.S. (2015), "Experimental investigation of frictional behavior between cohesive soils and solid materials using direct shear

apparatus", *Geotech. Geol. Eng.*, **34**(2), 567-578, http://doi.org/10.1007/s10706-015-9966-5.
Fukuoka, H., Sassa, K., Wang, G. and Sasaki, R. (2006), "Observation of shear zone development in ring-shear apparatus with a transparent shear box", *Landslides*, **3**(3), 239-251. http://doi.org/10.1007/s10346-006-0043-2.
Grelle, G. and Guadagno, F.M. (2010), "Shear mechanisms and viscoplastic effects during impulsive shearing", *Géotechnique*, **60**(2), 91-103. http://doi.org/10.1680/geot.8.p.019.
Han, W.J., Kim, S.Y., Lee, J.S. and Byun, Y.H. (2019), "Friction behavior of controlled low strength material-soil interface", *Geomech. Eng.*, **18**(4), 407-415. http://doi.org/10.12989/gae.2019.18.4.407.
Heidemann, M., Bressani, L.A. and Flores, J.A. (2020), "Residual shear strength of a residual soil of granulite", *Soils Rocks*, **43**(1), 31-41. http://doi.org/10.28927/SR.431031.
Hicher, P., Wahyudi, H. and Tessier, D. (1995), "Microstructural analysis of strain localisation in clay", *Int. J. Rock Mech. Min. Sci. Geomech.*, **31**(1), A26. http://doi.org/10.1016/0148-9062(95)90196-5.
Hoyos, L.R., Velosa, C.L. and Puppala, A.J. (2011), "A servo/suction-controlled ring shear apparatus for unsaturated soils: Development, performance, and preliminary results", *Geotech. Test. J.*, **34**(5), 1-11. http://doi.org/10.1520/GTJ103598.
Jiang, Y., Wang, G. and Kamai, T. (2016), "Fast shear behavior of granular materials in ring-shear tests and implications for rapid landslides", *Acta Geotech.*, **12**(3), 645-655. http://doi.org/10.1007/s11440-016-0508-y.
Khosravi, M., Meehan, C., Cacciola, D. and Khosravi, A. (2013), "Effect of fast shearing on the residual shear strengths measured along pre-existing shear surfaces in kaolinite", *Proceedings of the Geo-Congress*, San Diego, California, U.S.A., March.
Kimura, S., Nakamura, S., Vithana, S.B. and Sakai, K. (2013), "Shearing rate effect on residual strength of landslide soils in the slow rate range", *Landslides*, **11**(6), 969-979, http://doi.org/10.1007/s10346-013-0457-6.
Lee, S., Chang, I., Chung, M.K., Kim, Y. and Kee, J. (2017), "Geotechnical shear behavior of Xanthan Gum biopolymer treated sand from direct shear testing", *Geomech. Eng.*, **12**(5), 831-847, http://doi.org/10.12989/gae.2017.12.5.831.
Lemos, L.J.L. and Vaughan, P.R. (2000), "Clay-interface shear resistance", *Géotechnique*, **50**(1), 55-64. http://doi.org/10.1680/geot.2000.50.1.55.
Li, D., Yin, K., Glade, T. and Chin, L. (2017), "Effect of over-consolidation and shear rate on the residual strength of soils of silty sand in the Three Gorges Reservoir", *Sci. Rep.*, **7**, 5503, https://doi.org/10.1038/s41598-017-05749-4.
Li, Y.R. and Aydin, A. (2013), "Shear zone structures and stress fluctuations in large ring shear tests", *Eng. Geol.*, **167**, 6-13. http://doi.org/10.1016/j.enggeo.2013.10.001.
Li, Y.R., Aydin, A., Xu, Q. and Chen, J. (2012), "Constitutive Behavior of binary mixtures of kaolin and glass beads in direct shear", *KSCE J Civ. Eng.*, **16**(7), 1152-1159. http://doi.org/10.1007/s12205-012-1613-6.
Lupini, J.F., Skinner, A.E. and Vaughan, P.R. (1981), "The drained residual strength of cohesive soils", *Géotechnique*, **31**(2), 181-213. http://doi.org/10.1680/geot.1981.31.2.181.
Mamen, B., Kolli, M., Ouedraogo, E., Hamidouche, M., Djoudi, H. and Fanttozi, G. (2018) "Experimental characterisation and numerical simulation of the thermomechanical damage behaviour of kaolinitic refractory materials", *J. Australian Ceramic Soc.*, **55**, 555-565. | http://doi.org/10.1007/s41779-018-0262-8.
Mandl, G., de Jong, L.N.J. and Maltha, A. (1977), "Shear zones in granular material—an experimental study of their structure and mechanical genesis", *Rock Mech.*, **9**, 95-144. http://doi.org/10.1016/0148-9062(77)90973-1.
Meehan, C.L., Brandon, T.L. and Duncan, J.M. (2007), "Measuring drained residual strengths in the Bromhead ring shear", *Geotech. Test. J.*, **30**(6), 466-473. http://doi.org/10.1520/GTJ101017.
Morgenstern, N. and Tchalenko, J.S. (1969), "Microscopic structures in kaolin subjected to direct shear", *Geotechnique*, **19**(3), 426-327. http://doi.org/10.1680/geot.1969.19.3.426.
Sadrekarimi, A. and Olson, S.M. (2010), "Particle damage observed in ring shear tests on sands", *Can. Geotech. J.*, **47**(5), 497-515. http://doi.org/10.1139/t09-117.
Srivastava, D.K., Sahu, V. and Raghavendra, H.B. (2020), "Forensic study of slope failure case during heavy rainfall: Suggested preventative and remedial measures", *Geotech. Geol. Eng.*, **38**, 3697-3707. https://doi.org/10.1007/s10706-020-01247-z.
Suzuki, M., Van Hai, N. and Yamamoto, T. (2017), "Ring shear characteristics of discontinuous plane", *Soils Found.*, **57**(1), 1-22, https://doi.org/10.1016/j.sandf.2017.01.001.
Takizawa S., Kamai T. and Matsukura Y. (2005), "Fluid pathways in the shearing zones of kaolin subjected to direct shear tests", *Eng. Geol.*, **78**, 135-142, http://doi.org/10.1016/j.enggeo.2004.12.002.
Thakur, V. (2007), "Strain localization in sensitive soft clays", Ph.D. Dissertation, Norwegian University of Science and Technology, Trondheim, Norway.
Torabi, A., Braathen, A., Cuisiat, F. and Fossen, H. (2007), "Shear zones in porous sand: Insights from ring-shear experiments and naturally deformed sandstones", *Tectonophysics*, **437**(1-4), 37-50. http://doi.org/10.1016/j.tecto.2007.02.018.
Tsubakihara, Y., Kishida, H. and Nishiyima, T. (1993), "Friction between cohesive soils and steel", *Soils Found.*, **33**(2), 145-146. http://doi.org/10.1016/0148-9062(94)92910-6.
Wafid Agung, M., Sassa, K., Fukuoka, H. and Wang, G. (2004), "Evolution of shear-zone structure in undrained ring-shear tests", *Landslides*, **1**, 101-112. https://doi.org/10.1007/s10346-004-0001-9.
Wan, Y. and Kwong, J. (2002), "Shear strength of soils containing amorphous clay-size materials in a slow-moving landslide", *Eng. Geol.*, **65**(4), 293-303. http://doi.org/10.1016/s0013-7952(01)00139-9.
Wang, F., Sassa, K. and Wang, G. (2002), "Mechanism of a long-runout landslide triggered by the August 1998 heavy rainfall in FukushimaPrefecture", *Eng. Geol.*, **63**(1-2), 169-185. http://doi.org/10.1016/s0013-7952(01)00080-1.
Wang, L., Han, J., Yin, X. and Songyang, L. (2020), "Effect of moisture content and shearing speed on shear zone structure in fine-grained soils at large displacement", *Arab. J. Geosci.*, **13**(6), 1-11. https://doi.org/10.1007/s12517-020-5237-8.
Wei, H., Zhao, T., He, J., Meng, Q. and Wang, X. (2018), "Evolution of particle breakage for calcareous sands during ring shear tests", *Int. J. Geomech.*, **18**(2), 04017153, http://doi.org/10.1061/(ASCE)gm.1943-5622.0001073.
Wu, X. and Yang, J. (2017), "Tests of the interface between structures and filling soil of mountain area airport", *Geomech. Eng.*, **12**(3), 399-415. http://doi.org/10.12989/gae.2017.12.3.399.
Xu, C., Wang, X., Lu, X., Dai, F. and Jiao, S. (2018), "Experimental study of residual strength and the index of shear strength characteristics of clay soil", *Eng. Geol.*, **233**, 183-190. http://doi.org/10.1016/j.enggeo.2017.12.004.

GC